Inter-Cell Interference Coordination and Synchronization based on Location Information

Loïc Brunel, Mélanie Plainchault, Nicolas Gresset,
Armin Dammann, Christian Mensing, and Ronald Raulefs

***Abstract*—Mobile terminal location is an information which is available in mobile cellular systems. Location-based inter-cell interference coordination and synchronization are studied here for the 3GPP Long Term Evolution mobile cellular system. The impact of positioning inaccuracy is also evaluated.**

***Index Terms*—Positioning, inter-cell interference coordination, synchronization, multi link, 3GPP-LTE.**

I. Introduction

The location of mobile terminals is an information which is now available in mobile cellular systems, at the mobile terminal itself but also at its serving base station. The location information is either obtained from global navigation satellite systems (GNSS) or directly from the radio access of the mobile cellular system. In this paper, using the concrete example of the 3GPP Long Term Evolution (LTE) mobile cellular system, we study two aspects of the radio communications, which can take benefit from the positioning information: the inter-cell interference coordination (ICIC) and the synchronization. Section II presents location-based ICIC, where the location information is used at the base station and section III treats synchronization, where the location information is used at the mobile terminal. The impact of positioning inaccuracy is evaluated in both sections.

II. Inter-Cell Interference Coordination

A. Coordination Principle

The improvement of cell-edge throughput is an important target in recently designed mobile cellular networks with frequency reuse 1, like LTE [1]. Indeed, cell-edge users or user equipments (UEs) suffer from a strong inter-cell interference, especially in interference-limited scenarios with low inter-site distance. Since a trend is to reduce the cell size, it becomes crucial to control the inter-cell interference in order to achieve better cell-edge throughput. Furthermore, operators would like to provide a more homogeneous service, with better balanced cell-edge and cell-center throughputs.

Fig. 1 representing two neighboring cells, served by base stations (BS) BS_1 and BS_2, illustrates how the inter-cell interference impacts the signal-to-interference-plus-noise (SINR) level. UE_1 communicating with BS_1 is a cell-edge UE, receiving a weak useful signal S_1 and a strong interference I_1 from the neighboring BS_2. On the other hand, UE_2, also communicating with BS_1, is a cell-center UE, receiving a strong useful signal S_2 and a weak interference I_2. Thus, UE_1 experiences a low SINR whereas UE_2 benefits from a high SINR. It results in strong throughput disparities among UEs. The main purpose of inter-cell interference coordination (ICIC) is to reduce these disparities. However, a major issue when applying ICIC is the difficulty to anticipate the interference level. Indeed, it depends on the actual time-varying scheduling in neighboring cells. In LTE, for instance, the time domain is divided into sub-frames of 1ms, which represent the time scheduling granularity. The LTE multiple access scheme is the orthogonal frequency division multiple access (OFDMA), in which each UE is allocated a part of the bandwidth during a sub-frame. Thus, the interference experienced by a UE in a given sub-frame may be very different from the interference experienced for the same frequency allocation in the following sub-frame. This is why radio resource planning is needed among neighboring cells in order to coordinate inter-cell interference on a long-term basis. The radio resource planning may be fixed or may vary in time thanks to some signaling between BSs as in LTE. In this paper, we focus on a fixed intra-band frequency planning with

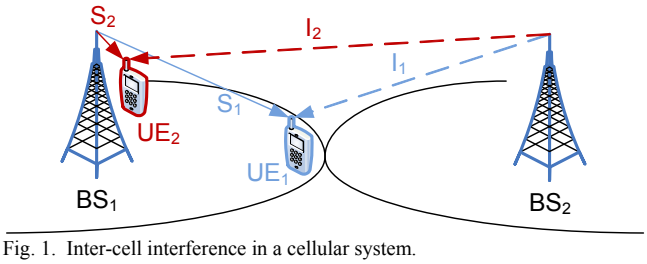

Fig. 1. Inter-cell interference in a cellular system.

with three cell types C_1, C_2, C_3 as depicted in Fig. 2 for an hexagonal deployment of 7 BSs with 3 sectors. We use here the LTE terminology: a cell is a sector of a BS.

A given cell type, corresponding to a given power pattern, varying in frequency but fixed in time, is associated to each cell. The cell type C^i is chosen for a given cell i in such a way that all its neighboring cells have a cell type different from C^i.

L. Brunel, M. Plainchault and N. Gresset are with Mitsubishi Electric R&D Centre Europe, 1 allée de Beaulieu – CS 10806, 35708 Rennes Cedex 7, France (e-mails: {l.brunel, m.plainchault, n.gresset}@fr.merce.mee.com).

A. Dammann, C. Mensing and R Raulefs are with the Institute of Communications and Navigation, German Aerospace Center (DLR), Oberpfaffenhofen, 82234 Wessling, Germany (e-mails: {Armin.Dammann, Christian.Mensing, Ronald.Raulefs}@DLR.de).

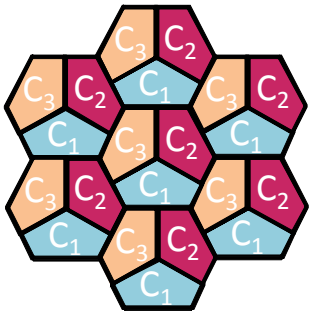

Fig. 2. Planning with three cell types C_1, C_2, C_3.

There exist different techniques of interference coordination, depending on the pre-defined power pattern and the coordination strategy. Some of them are illustrated in Fig. 3. We study different approaches taking into account the impact of UE location knowledge on the ICIC performance. The positioning information can be directly used for ICIC or be an entry for a fingerprinting map.

B. *Hard Frequency Reuse*

With the so-called hard frequency reuse strategy, signals of neighboring cells are transmitted in non-overlapping frequency sub-bands. With three cell types, each cell is allocated a third of the system bandwidth, which by definition results in a frequency reuse factor 3. The throughput is increased by the SINR improvement resulting from the interference mitigation. Unfortunately, it is also limited by the partial bandwidth usage which induces both a direct division of the spectral efficiency by a factor 3 and a degraded performance due to larger restrictions on the frequency scheduling.

C. *Partial Frequency Reuse*

In order to circumvent the drawbacks of the hard reuse strategy, the so-called partial frequency reuse [2] applies a frequency reuse factor 3 (with the 3 cell-types' example) on a part of the bandwidth and a frequency reuse factor 1 on the rest of the bandwidth. Cell-edge UEs are scheduled in the part of the bandwidth with frequency reuse 3, where they experience a limited interference. However, they suffer from the drawbacks of hard frequency reuse. Thus, the performance of partial frequency reuse lies between the performance of hard frequency reuse and the performance without ICIC. The lower the proportion of UEs in hard reuse is, the closer to the no ICIC case the partial reuse performs.

D. *Soft Frequency Reuse*

In order to avoid the spectral efficiency division when using a frequency reuse factor 3, soft frequency reuse has been introduced [3][4]. In each cell, a large maximum transmission power P_{max} is allowed in a single sub-band, whereas only a limited maximum transmission power P_{min} is allowed in the two other sub-bands. We denote β the ratio P_{min} / P_{max}. Based on this long-term power frequency planning, the BS is able to perform an efficient scheduling in order to increase the cell-edge throughput, at the expense of the average throughput.

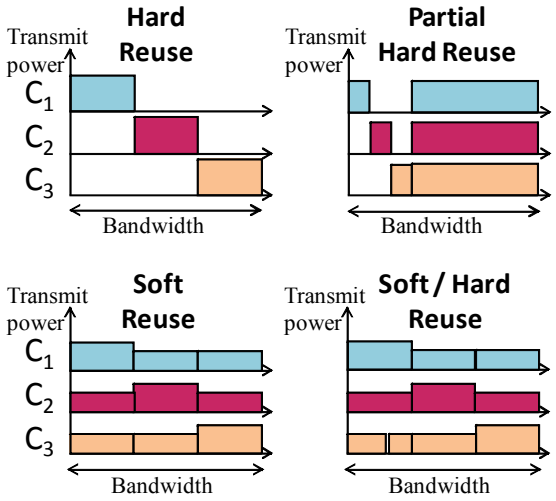

Fig. 3. Different power patterns used for ICIC.

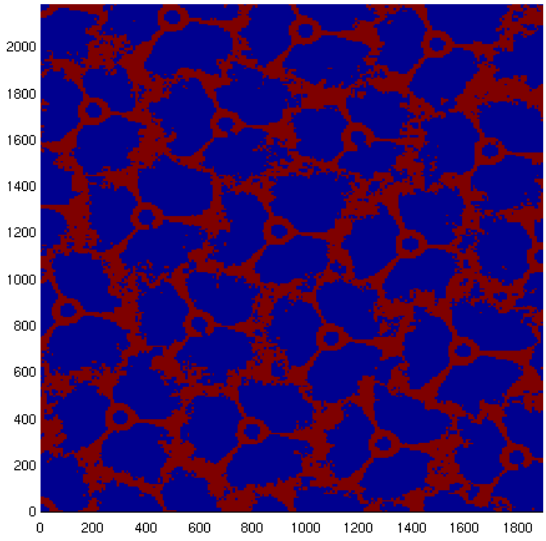

Fig. 4. Fingerprinting map of UE states for long-term classification.

Cell-edge UEs are scheduled on the sub-band with improved SINR, i.e., the sub-band with transmission power P_{max} and lowest experienced interference, whereas cell-enter UEs are scheduled in the two other sub-bands.

The choice of β impacts performance. When β decreases from 1, the cell-edge performance is first improved. Then, β becomes so low that original cell-center UEs are so degraded that they have a spectral efficiency lower than original cell-edge UEs and the performance starts to decrease. Thus, there is an optimal β value.

The scheduler must first determine if a UE is a cell-edge UE or a cell-center UE. We investigate two types of classification. In the *long-term classification*, UEs, which belong to the third of UEs with lowest long-term SINR, are classified as cell-edge UEs. Fast fading is not taken into account here. In *short-term classification*, the frequency-selective fast fading is included in the SINR evaluation. This

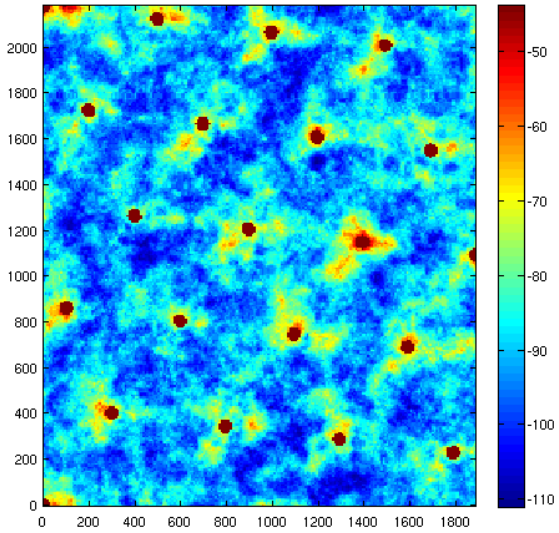

Fig. 5. Fingerprinting map of inter-cell interference (in dB).

more accurate classification further improves the cell-edge throughput.

Use of location information

There is a clear relationship between the long-term SINR level and the UE location without shadowing. The SINR level depends on the neighboring BSs' positions, which should be made available. However, a shadowing with a strong variance makes the location information irrelevant [5].

With shadowing and long-term classification, a fingerprinting map containing the UE state (cell-edge or cell-center) for a given position may be used for long-term classification. Such a fingerprinting map is shown in Fig. 4, where red points are cell-edge positions and blue points are cell-center positions. With such a map, shadowing is efficiently taken into account, especially because it is spatially correlated. The expected advantage of using the location information is low complexity. Once the fingerprinting map has been built, the scheduler directly knows if the UE is a cell-edge UE or a cell-center UE from its position. It does not have to accumulate short-term SINR values reported by the UE to compute the long-term SINR before deciding if the UE is a cell-edge UE or not.

For short-term classification, a fingerprinting map containing the experienced long-term interference can be used together with the instantaneous power received by the UE from its serving BS. The latter power is obtained at the UE by channel estimation and reported to the BS. An example of inter-cell interference fingerprinting map is shown in Fig. 5.

Obviously, the relevance of the fingerprinting maps depends on the location accuracy and the fingerprinting map spatial granularity. It also depends on the interference level quantization for interference maps.

TABLE I
SIMULATED DOWNLINK LTE SYSTEM

Carrier frequency	2 GHz
System bandwidth	5 MHz
Sampling frequency	7.68 MHz
Modulation scheme	OFDM
Sub-carrier spacing	15 kHz
FFT length	512
Number of modulated sub-carriers	300
Number of OFDM symbols per sub-frame	14
Modulation and coding schemes (MCS)	No explicit MCS: Shannon capacity evaluation
UE allocation size	1 physical resource block (PRB) pair, i.e., 12 sub-carriers (180 kHz) × 14 OFDM symbols
Perfect scheduling	Each user is allocated the best PRB assuming that there is not any latency issue
Restrictions	No mobility scenario, no handover, no traffic model, no power control

TABLE II
DEPLOYMENT PARAMETERS

Hexagonal layout with wrap-around	19 sites, 3 sectors per site
BS antenna	Sectorized BS antenna [6]
UE antenna	Omni-directional UE antenna
Inter-site distance	500 m
BS transmit power	43 dBm
UE noise factor	9 dB
Penetration loss	20 dB
Path-loss model	LTE macro-cell Hata model: $128.1 + 37.6\log_{10}(d_{km})$ [dB]
BS antenna height	15 m
Lognormal shadowing	8dB variance, 50m correlation distance
Channel model	1x2 Typical Urban channel Delays: 0 0.2 0.5 1.6 2.3 5 µs Mean powers: -3, 0, -2, -6, -8, -10 dB

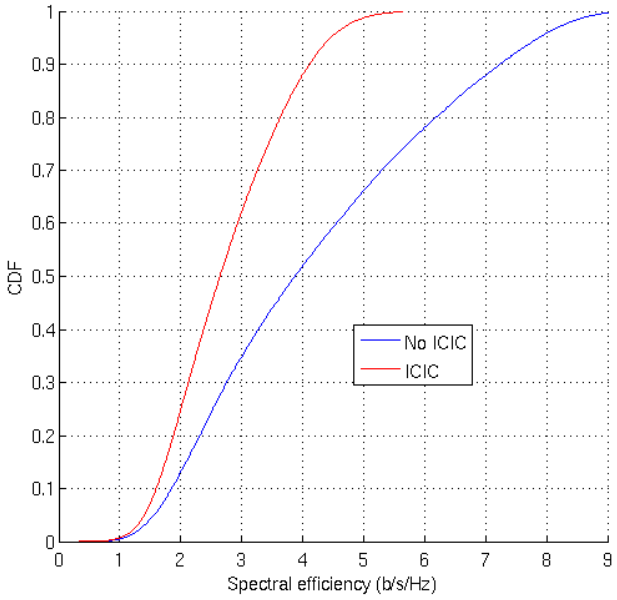

Fig. 6. Performance of hard frequency reuse.

E. Soft / Hard Reuse

Due to the overlapping of the antenna patterns of the

different sectors of a same BS, UEs located at the boundary between two sectors suffer from a poor SINR even if their useful signal is strong. Thus, joint scheduling can be used between two sectors of a same BS in addition to soft frequency reuse. As depicted in Fig. 3, the joint scheduler makes sure that the resource used by a UE close to the boundary between two sectors is not used in the interfering sector. These UEs can be easily identified by positioning, even with shadowing. Indeed, in a urban environment, where the scatterers are not far, the shadowing can be assumed to be the same for both the useful and the interfering signals. Thus, UEs located at the sector boundary, close to the base station, experience an interference from the neighboring sector which has the same level as the useful signal. Positioning also helps in identifying the most interfering sector. Performing joint scheduling for two sectors of a same BS is much easier than joint scheduling between two BSs.

F. Simulation results

The different ICIC techniques are compared using a static multi-cell system simulator. The layout is hexagonal with wrap around. Multiple UEs are dropped uniformly and associated to the BS with best path gain. We evaluate the ICIC performance for a LTE system with 3 sub-bands. For techniques involving soft-frequency reuse, β is optimized and set to 0.3. The main parameters of the downlink system level evaluation performed for this study are listed in Tables I and II. The inter-site distance is chosen to be relatively low in order to simulate an interference-limited scenario. The same total transmission power is kept for all simulated techniques. We compare the average throughput and the cell-edge throughput (5-percentile throughput) of the different methods and the impact of location error. The location error is modeled as a uniformly distributed error in a circle with the maximum position error as radius.

The cell-edge throughput and the average throughput without ICIC are 1.56 b/s/Hz and 4.21 b/s/Hz, respectively.

Fig. **6** shows the strong throughput degradation, especially for cell-center UEs brought by hard frequency reuse compared to a system without ICIC. The obtained cell-edge and average throughputs are only 1.4 b/s/Hz and 2.76 b/s/Hz, respectively.

Fig. 7 shows the gain brought by soft frequency reuse even with long-term classification. The cell-edge throughput is increased to 1.97 b/s/Hz (26% gain) at the expense of a small average throughput 8% decrease down to 3.89 b/s/Hz. When using a fingerprinting map on UE states, with a maximum position error of 10 m, ICIC still performs well. However, with a 50m maximum error, it is preferable not to apply ICIC since the cell-edge throughput is not improved and the average throughput is degraded. Indeed, the UE classification becomes erroneous and useless constraints are applied to the scheduling.

With short-term classification, in Fig. 8, the cell-edge throughput becomes higher (2.11 b/s/Hz, 35% gain) at the expense of a smaller average throughput decrease (7%, 3.91 b/s/Hz). The same degradation as with long-term

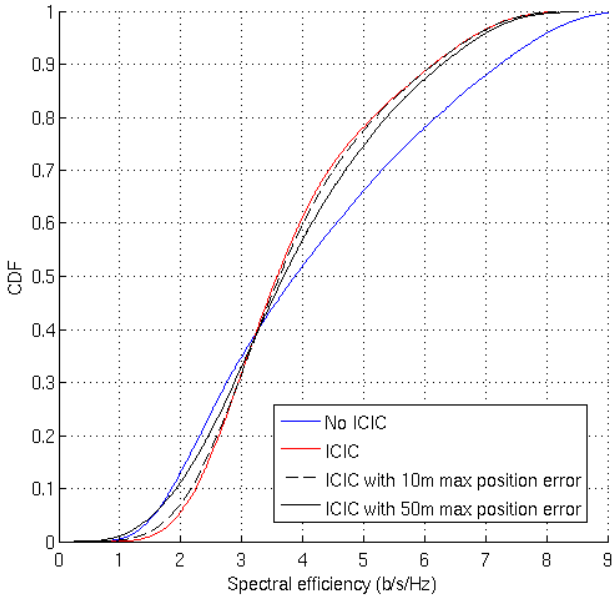

Fig. 7. Performance of soft frequency reuse with long-term UE classification.

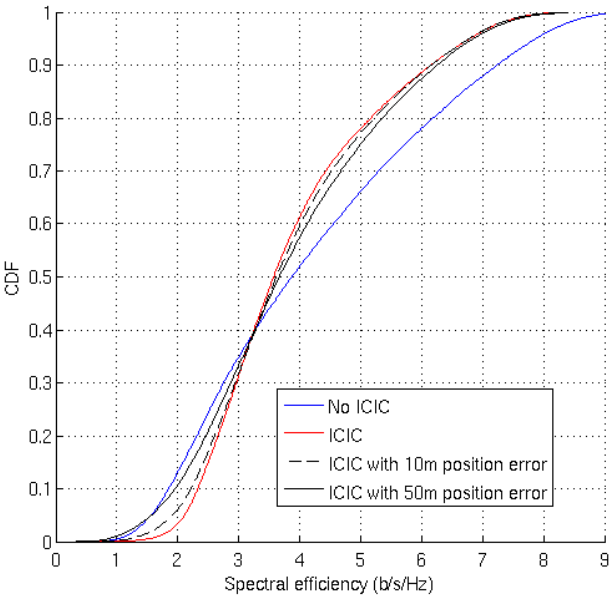

Fig. 8. Performance of soft frequency reuse with short-term UE classification.

classification is observed when erroneous location information is used.

Finally, Fig. 9 presents the performance of soft/hard reuse. The cell-edge and average throughputs are lower than with soft frequency reuse (1.97 b/s/Hz and 3.91 b/s/Hz, respectively). This lower performance is confirmed with location errors. Soft / hard reuse suffers from the spectral efficiency decrease resulting from the unused resources, just as hard reuse, even if the scheduling constraint does exist for soft / hard reuse.

The performance results for the different investigated techniques show that the positioning error should be lower than 50 m, the shadowing correlation distance, in order to allow efficient location-based ICIC.

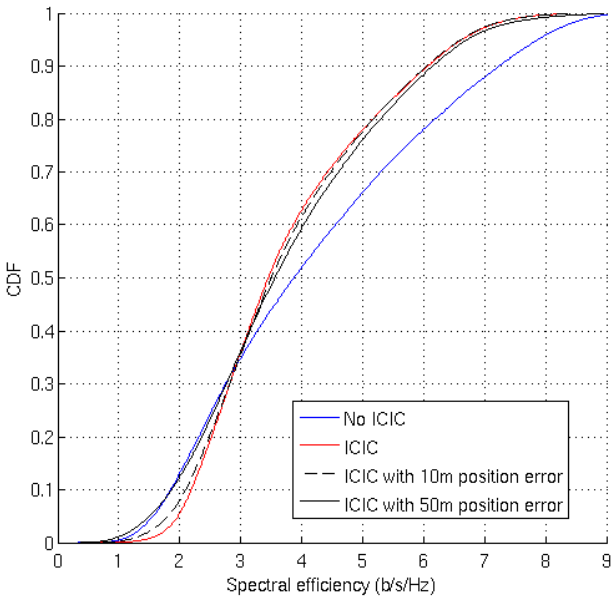

Fig. 9. Performance of soft / hard frequency reuse with short-term UE classification.

III. Location Based Iterative Synchronization for Cellular OFDM

In this section, we investigate potential time synchronization performance gains resulting from the exploitation of location and channel state information. The evaluation is based on the beyond 3G standard 3GPP-LTE. We first introduce the relevant aspects of the 3GPP-LTE specification for synchronization investigations. We introduce appropriate synchronization methods and extend them for multi-link synchronization. To some extent the proposed methods are related to the concept of macro diversity for data modulation since they exploit signal energy from different transmission sites. Simulations using a typical urban multi-cell scenario show the achievable performance of the proposed time synchronization methods with focus on operation at the critical cell edge.

A. System Description

The physical layer of the 3GPP-LTE downlink is basically a coded OFDM system. Different logical channels are encoded using a turbo- or convolutional code. The coded bits are interleaved and modulated onto BPSK, QPSK, 16- or 64-QAM symbols. Data and pilot symbols are multiplexed into OFDM symbols. For details about channel coding, modulation, scrambling, interleaving, precoding, spatial signal processing, etc., we refer to the respective standard documents [7][8][9]. The focus of this section is on time synchronization, so we are interested in those signal parts of 3GPP-LTE, which are dedicated for timing estimation. Subsequently, we briefly introduce the 3GPP-LTE framing structure which embeds the synchronization sequences we are interested in for our investigations.

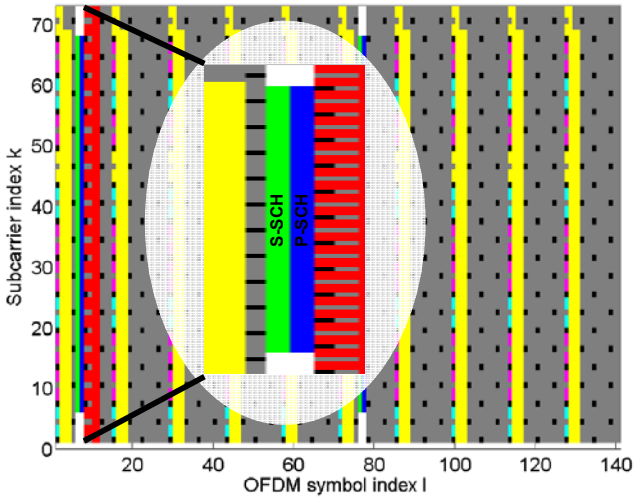

Fig. 10. 3GPP-LTE frame structure for the core subcarriers of the spectrum. Mapping of physical channels to resource elements: Primary Synchronization Channel (P-SCH), Secondary Synchronization Channel (S-SCH), Cell Specific Reference Signal (Pilots), Physical Control Format Indicator Channel (PCFICH), Physical Hybrid ARQ Indicator Channel (PHICH), Physical Downlink Control Channel (PDCCH), Physical Broadcast Channel (PBCH), Physical Downlink Shared Channel (PDSCH).

1) 3GPP-LTE Frame Structure

Generally, there are two different types of 3GPP-LTE radio frames, applicable to frequency division duplex ("Type 1") and time division duplex ("Type 2"). We are focusing on the FDD frame "Type 1". Such a radio frame is 10 ms long and consists of 10 subframes. Each of them is built from two so-called slots. So, each downlink slot has a length of 0.5 ms and consists of 3, 6 or 7 OFDM symbols, dependent on the cyclic prefix length mode and the subcarrier spacing f_{SC}, i.e., the core OFDM symbol length

$$T_{OFDM} = \frac{1}{f_{SC}} = \frac{1}{15\ \text{kHz}} = 66.67\ \mu\text{s}\cdot \quad (1)$$

Note, there is an optional subcarrier spacing of f_{SC} = 7.5 kHz, which reduces the guard interval overhead but is more sensitive against Doppler.

Fig. 10 shows the frame structure for the 72 core subcarriers of the spectrum containing synchronization signals and control channels. The different physical channels are

- Primary Synchronization Channel (P-SCH, blue),
- Secondary Synchronization Channel (S-SCH, green),
- Cell Specific Reference Signal (Pilots, black),
- Physical Control Format Indicator Channel (PCFICH, cyan),
- Physical Hybrid ARQ Indicator Channel (PHICH, magenta),
- Physical Downlink Control Channel (PDCCH, yellow),
- Physical Broadcast Channel (PBCH, red),
- Physical Downlink Shared Channel (PDSCH, gray).

3GPP-LTE supports 1.4, 3, 5, 10, 15 and 20 MHz channel bandwidths, which correspond to 72, 180, 300, 600, 900 and

1200 actively used OFDM subcarriers [7].

a) Primary Synchronization Channel

There are three different P-SCH sequences which are generated from frequency-domain Zadoff-Chu sequences of length 62. These 62 symbols are mapped to the central subcarriers of the last OFDM symbol in slot 0 and 10 of an LTE Type 1 radio frame [10]. Two of the sequences have the same magnitude and only differ in the phase. The P-SCH sequences can be used to estimate the integer and fractional frequency offset in the receiver [12][15]. Because there are only three sequences, a bank of matched filters can be used for precise timing estimation [20].

b) Secondary Synchronization Channel

In total, there are 504 different S-SCH sequences, which are grouped into 168 unique physical layer cell identity groups, each containing 3 cell identities. The cell identity within each group is indicated by the P-SCH, whereas the S-SCH signal carries the cell identity group number. For the generation of S-SCH sequences two length 31 binary m-sequences are interleaved. Each of the resulting 168 sequences is scrambled by one of 3 length 31 m-sequences, determined by the P-SCH signal, i.e., the cell identity. The 62 binary frequency-domain samples are mapped to the central subcarriers of the one before the last OFDM symbol in slot 0 and 10 of an LTE Type 1 radio frame, i.e., they appear prior to the P-SCH. Thus, it is possible to detect the start of the S-SCH sequences with a reverse differential correlation [12]. Although this approach may be less accurate than the matched filter correlator bank for the P-SCH, it has the benefit of being robust against frequency offsets. As the sequences between slot 0 and slot 10 differ, the S-SCH pilot can be used to detect the frame start.

2) Channel Model

For our simulations we need a channel model which provides multiple-link capabilities. Such capabilities are provided by channel models, developed during the EU-Project WINNER [14][21]. The WINNER models are based on clusters of scatterers for multipath modeling. Besides small scale fading, i.e., frequency selective fading, these models also cover large scale effects like

- Delay spread/distribution,
- Angle of departure spread/distribution,
- Angle of arrival spread/distribution,
- Shadow fading,
- Rice factor.

The parameters of these effects strongly depend on the propagation environment and have been modeled for a variety of environmental scenarios. Parameters, supported by the WINNER models are

- Scaling of delay distribution,
- Cross polarisation,
- Number of clusters,
- Cluster angle spread of arrival/departure,
- Per cluster shadowing,
- Autocorrelation of large scale parameters,
- Crosscorrelation of large scale parameters,
- Number of rays per cluster.

For our simulations, we use the "WINNER C2 Typical Urban" channel model [14]. This model describes a typical urban macro cell for mobile velocities of 0-120 km/h and carrier frequencies in the range of 2-6 GHz. In this scenario, the mobile station is located outdoors at street level. It provides a mixture of line-of-sight (LOS) and non-LOS propagation conditions, where the LOS probability depends on the distance between mobile and base station. The LOS/NLOS propagation condition state of a link itself influences further parts of the model like the path loss model for instance.

B. Synchronization

Symbol or frame timing and carrier frequency offset estimation/correction are two tasks, which have to be performed prior to any data detection, demodulation and decoding. Synchronization algorithms are usually based on knowledge at the receiver about parts of the transmitted signal, i.e., the synchronization sequences. Using correlation methods, this knowledge can be exploited to find the beginning of the synchronization sequences within the received signal or the frequency offset of the local receiver oscillator.

1) Cross Correlation

Timing estimation can be performed using complete knowledge about the transmitted synchronization sequences. For that we compare the received signal $r(k)$ by cross correlation

$$CC(n) = \sum_{k=0}^{N-1} s(k)\, r^*(k+n), \tag{2}$$

with the transmitted reference synchronization signal $s(k)$. Note, this method is not robust against carrier frequency offsets. Unlike differential correlation, a carrier frequency offset term remains in the correlation sum in Equation (2) and, thus, leads to a degradation of auto- and cross-correlation properties of the applied synchronization sequences. Nevertheless, we use the cross-correlation method for timing synchronization in order to take into account auxiliary information about the location of the mobile and the channel state. Therefore we use a multi-link model for the received signal

$$r(k) = \sum_{i=1}^{N_{\mathrm{BS}}} \alpha_i(k, d_i)\, s_i(k) * \alpha_i(k - \delta_i) + n(k). \tag{III.3}$$

which is a superposition of N_{BS} signals, transmitted from adjacent base stations (BSs). Here, $s_i(k)$ denotes the signal, transmitted from BS i, i.e., the 3GPP-LTE radio frames, containing the P-SCH and S-SCH sequences. $h_i(k-\delta_i)$ is the channel impulse response from BS i to the mobile station (MS), taking into account the absolute signal travelling time δ_i (in samples). "*" denotes the convolution operation. We assume that the average energy of the channel impulse (small

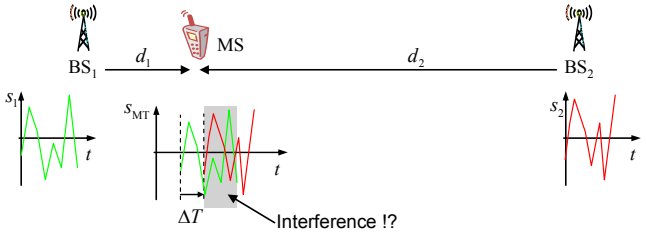

Fig. 11. Location aware synchronization.

scale fading) $h_i(k)$ is normalized to one, i.e., $\sum_k \mathrm{E}\left\{\left|h_i(k)\right|^2\right\}=1$. Large scale fading effects like shadow fading and path loss are described by the factor $\alpha_i(k,d_i)$, which is time variant and dependent on the distance d_i between BS i and the MS. We assume that the distances $d_i = cT_{\mathrm{samp}}\delta_i$ are proportional to the signal travelling times δ_i. $n(k)$ denotes additive white Gaussian noise with variance $\sigma^2=\mathrm{E}\left\{\left|n(k)\right|^2\right\}$.

2) Multi-Link Synchronization — The usage of Location Information

As mentioned at the beginning, there are high interference levels at the cell edges of a cellular communications system with a frequency reuse of one. Signals coming from different BSs superimpose at the cell border with similar power levels. It is straightforward to raise the question, whether we can use signal energy of synchronization signals received from different BSs. Fig. 11 points out the situation and the proposed approach — which is very much related to the principle of macro diversity — for two BSs. Signals s_1 and s_2 are transmitted synchronously from a serving BS_1 and an adjacent BS_2. Because of different signal propagation delays δ_1 and δ_2 they arrive at the MS with a time shift $\Delta T = \delta_1 - \delta_2$. If nothing is known about the signal s_2, this signal hits the signal of the serving BS as interference. However, synchronization sequences are usually known. Dependent on the distances d_1 and d_2 the time shift

$$\Delta T = \delta_2 - \delta_1 = \frac{d_2 - d_1}{c}. \tag{4}$$

can be calculated, where c is the speed of light. Consequently, ΔT is also the time shift of the correlation peaks obtained from two correlators which are matched to s_1 and s_2. Knowing the time shift ΔT the correlator output signals can be combined. Generally, we assume a bank of correlators

$$CC_i(n) = \sum_{k=0}^{N-1} s_i(k)\, r^*(k+n), \quad i = 1,\ldots,N_{\mathrm{BS}}, \tag{5}$$

which are matched to the synchronization sequences within radio frames $s_i(k)$, $i=1,\ldots,N_{\mathrm{BS}}$ transmitted from the N_{BS} base stations. For combining the correlator signals, we first have to shift them according to the time shifts

$$\delta_i = \frac{d_i}{cT_{\mathrm{samp}}}, \quad i = 1,\ldots,N_{\mathrm{BS}}. \tag{6}$$

denoted in samples. The MS- BS_i distances d_i are calculated from the positions of MS and BS_i. The positions of the BSs are fix and usually known. The MS position can be obtained by satellite navigation systems like GPS or by positioning

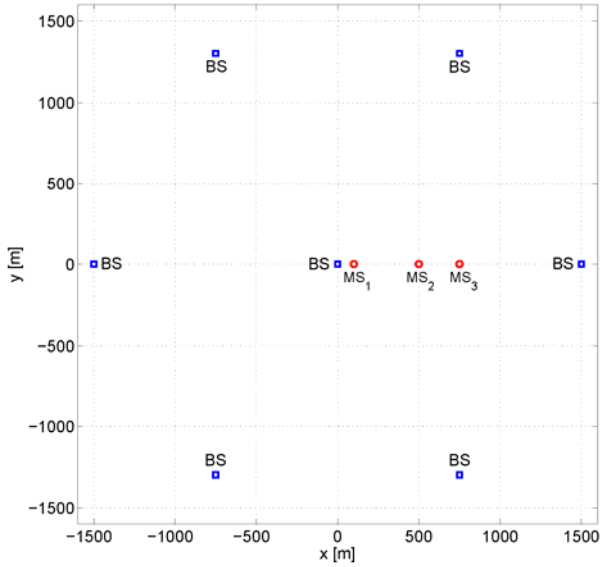

Fig. 12. Cellular simulation scenario.

within 3GPP-LTE itself. Simply summing up the magnitudes of the shifted correlators yields to the principle of equal gain combining (EGC). In order to take into account the quality of the signal, we weight the individual correlator outputs before summation. This approach is related to maximum ratio combining (MRC). Thus, we have

$$CC(n) = CC_i(n) = \sum_{i=1}^{N_{\mathrm{BS}}} \gamma_i \left| CC_i(n-\delta_i) \right|. \tag{7}$$

We obtain a timing estimate by searching for the maximum of that combination, i.e.,

$$\hat{n}_0 = \arg\max_n CC(n), \tag{8}$$

The weighting coefficients are

$$\gamma_i = \begin{cases} 1, & \text{EGC}, \\ \mathrm{SINR}_i, & \text{MRC}, \end{cases} \tag{9}$$

where we use the signal-to-interference-plus-noise ratios SINR_i as weighting coefficients. In our approach, the SNIRs are calculated from the long term fading factors $\alpha_i(k,d_i)$ by

$$\mathrm{SINR}_i = \frac{\left|\alpha_i(k,d_i)\right|^2}{\sigma^2 + \sum_{i\neq j}\left|\alpha_i(k,d_i)\right|^2} = \frac{\left|\alpha_i(k,d_i)\right|^2}{\mathrm{E}\left\{\left|r(k)\right|^2\right\} - \left|\alpha_i(k,d_i)\right|^2} \tag{10}$$

Here, we assume that $|\alpha_i(k,d_i)|^2$ represents the received signal power from BS_i without noise, i.e.,

$$\mathrm{E}\left\{\left|r(k)\right|^2\right\} = \sum_i \left|\alpha_i(k,d_i)\right|^2 + \sigma^2, \tag{11}$$

where σ^2 is the AWGN variance. Estimates of $\mathrm{E}\{|r(k)|^2\}$, $|\alpha_i(k,d_i)|^2$ and σ^2 can either be provided by an appropriate channel estimation algorithm or predicted by using a fingerprint database and the knowledge of the MS position, i.e., the distances d_i.

3) Channel State Information

Wireless communications systems have to cope with significant multipath propagation. Thus, replicas of the transmitted signal arrive at different time instances at the receiver. This results in a bias of the maximum magnitude of

the cross correlation functions as defined for instance in Equation (5). To get rid of this bias, we have to cross correlate the received signal $r(k)$ with the hypothetic signal right after multipath propagation. Therefore, we replace $s_i(k)$ in Equation (5) by $\tilde{s}_i(k) = s_i(k) * h_i(k)$. The channel impulse response $h_i(k)$ has to be provided by a channel estimation algorithm for each BS, which is taken into account for multi-link synchronization.

C. Results

For the evaluation of the benefit of location and channel state information, we use a cellular simulation environment setup as shown in Fig. 12. BSs are located in a hexagonal grid with a cell radius of of 750 m. We have applied the WINNER C2 Typical Urban multi-link channel model [14] with a BS TX power of 43 dBm. The MS is located at the cell edge at position MS_3 [x, y] = [750, 0] m. The MS speed is set to 2 m/s. The simulation results below show the timing accuracy as cumulative density functions (CDFs) over time samples for the S-SCH of 3GPP-LTE. One time sample corresponds to 32.55 ns. The carrier frequency offset for all the simulations is assumed to be zero.

For the investigation of the influence of location and channel state information we subsequently focus on CC. Fig. 13 compares the synchronization accuracy at the critical cell edge, taking into account location information according to Equation (7). For comparison we have redrawn the graph for the single-link synchronization performance of CC. There is a marginal improvement for MRC and EGC taking into account 2 BSs. The number of BSs which are taken into account for MRC does not show any significant influence. Using more than 2 BSs for EGC results in a performance degradation. Here, the more noisy correlation signals coming from BSs which are further apart compared to the 2 closest ones, are added with an inadequately high weight. The long term fading coefficients $|\alpha_i(k,d_i)|^2$ which are required for the calculation of the MRC weighting coefficients as well as the MS position are assumed to be perfectly known.

1) Usage of Channel State Information

In comparison to the previous results, Fig. 14 shows the performance improvements taking additionally into account the channel impulse response according to Sec. B.3). Compared to the single-cell synchronization performance, now multi-link synchronization provides performance improvements for both EGC and MRC. Further increasing the number of BSs for EGC does not improve the timing accuracy further. Because of combining too noisy signals, the performance again decreases for EGC if the number of involved BSs is becoming too high. As it can be expected, the performance of MRC is monotonically increasing with an increasing number of combined BSs.

Comparing the results, shown in Fig. 13 and Fig. 14, indicates that the multipath correlation bias significantly conceals potential gains resulting from the combination of synchronization signals transmitted from different BSs.

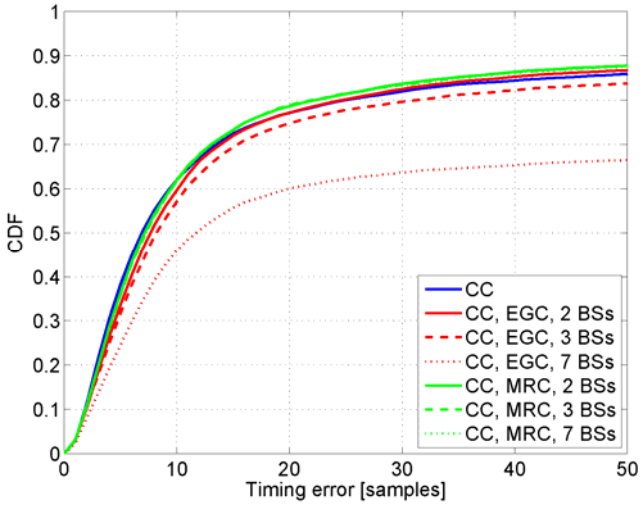

Fig. 13. Multi-link S-SCH synchronization accuracy at the cell border for cross correlation (CC) with equal gain combining (EGC) and maximum ratio combining (MRC) for the 2, 3 or 7 strongest BSs without knowledge of channel state information. One time sample corresponds to 32.55 ns.

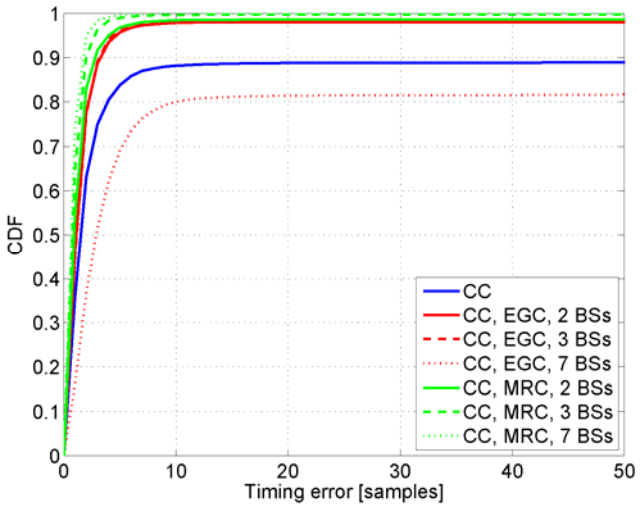

Fig. 14. Multi-link S-SCH synchronization accuracy at the cell border for cross correlation (CC) with equal gain combining (EGC) and maximum ratio combining (MRC) for the 2, 3 or 7 strongest BSs, taking into account channel state information.

2) Effect of imperfect Location Information

Previously, we have assumed that the position of the MS is perfectly known. Location information is required to calculate the timing offsets for correlation signal combination in Equation (7). However, there are inaccuracies, since the MS position has to be estimated in some appropriate way. In this section we are interested in the influence of location estimation errors on the performance of the location aware synchronization algorithms. Compared to previous results, we have modeled and introduced a location error as 2-dimensional Gaussian random process with zero mean and standard deviations of 10 m, 40 m and 100 m. In Fig. 15 results are drawn for MRC, including the 7 strongest BSs, with and without small scale channel state information (CSI),

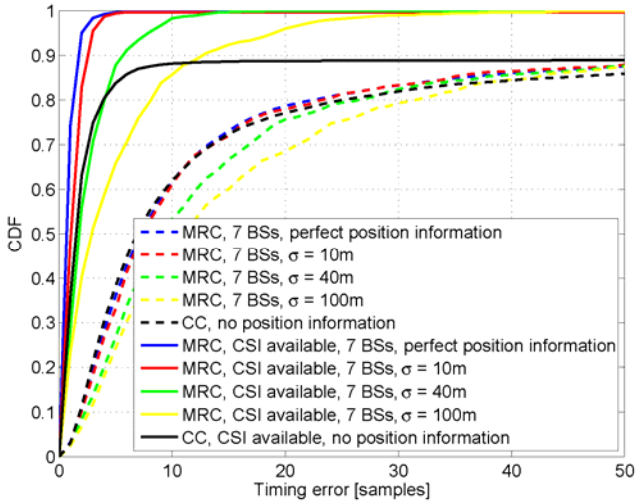

Fig. 15. The effect of location inaccuracy on S-SCH synchronization performance at the cell border for cross correlation (CC) with maximum ratio combining (MRC) for the 7 strongest BSs

i.e. the channel impulse response. For comparison the performance curves for single link synchronization (no position information) are shown. Without using CSI there is almost no performance gain. If there is a significant location error, the synchronization performance is degraded. Exploiting CSI results in synchronization performance gains as the localization error σ remains below 40 m. However, even for a relatively high localization error of σ = 100 m the performance graphs for multi link synchronization show an earlier approach to a probability of one compared to single link synchronization.

Simulation results shown above have shown timing performance gains if small scale fading information, i.e., the channel impulse response, is available and taken into account for correlations. Reversely, this means that timing degradations due to multipath propagation significantly conceal potential gains resulting from location aware multi-link synchronization. Therefore, the combination of location information and channel state information promises remarkable performance gains for high precision time synchronization requirements.

IV. Conclusion

Using location information reduces the complexity of ICIC, limiting the required amount of reporting from the mobile terminals thanks to the usage of fingerprinting maps at the base stations. The mobile terminal can also benefit from the location information for improving its synchronization performance by jointly using synchronization signals from several base stations. For both inter-cell interference coordination and purposes, a positioning accuracy in the range of 10 m to 20 m meters is required for performance improvements.

Acknowledgment

This work has been performed in the framework of the ICT project ICT-217033 WHERE, which is partly funded by the European Union.

References

[1] ETSI. LTE; Evolved Universal Terrestrial Radio Access (E-UTRA) and Evolved Universal Terrestrial Radio Access Network (E-UTRAN) (3GPP TS 36.300, version 8.11.0 Release 8), December 2009. ETSI TS 136 300 V8.11.0.

[2] M. Sternad, T. Ottosson, a. Ahlén, A. Svensson. Attaining both coverage and high spectral efficiency with adaptive OFDM downlinks. IEEE Vehicular Technology Conference (VTC), Orlando, October 2003.

[3] Y. Xiang, J. Luo, C. Hartmann. Inter-cell interference mitigation through flexible reuse in OFDMA based communication networks. European Wireless Conference, Paris, April 2007.

[4] Huawei. 3GPP R1-050841: Further analysis of soft-frequency reuse scheme. 3GPP TSG RAN WG1#42, London, August 2005.

[5] ICT-217033 WHERE. WHERE Deliverable D3.1: Physical layer enhancements using localization data, January 2009.

[6] ETSI. LTE; Further advancements for E-UTRA – Physical layer aspects (3GPP TR 36.814 version 1.5.0), November 2009.

[7] ETSI. LTE; Evolved Universal Terrestrial Radio Access (E-UTRA); Base Station (BS) radio transmission and reception (3GPP TS 36.104 version 8.6.0 Release 8), July 2009. ETSI TS 136 104 V8.6.0.

[8] ETSI. LTE; Evolved Universal Terrestrial Radio Access (E-UTRA); Long Term Evolution (LTE) physical layer; General description (3GPP TS 36.201 version 8.3.0 Release 8), April 2009. ETSI TS 136 201 V8.3.0.

[9] ETSI. LTE; Evolved Universal Terrestrial Radio Access (E-UTRA); Multiplexing and channel coding (3GPP TS 36.212 version 8.7.0 Release 8), June 2009. ETSI TS 136 212 V8.7.0.

[10] ETSI. LTE; Evolved Universal Terrestrial Radio Access (E-UTRA); Physical channels and modulation (3GPP TS 36.211 version 8.7.0 Release 8), June 2009. ETSI TS 136 211 V8.7.0.

[11] David Astély, Erik Dahlman, Anders Furuskär, Yiva Jading, Magnus Lindström, and Stefan Parkvall. LTE: The evolution of mobile broadband. IEEE Communications Magazine, 47(4):44–51, April 2009.

[12] F. Berggren and B. M. Popovic. A non-hierarchical cell search scheme. IEEE Wireless Communications and Networking Conference (WCNC), March 2007.

[13] J.-C. Belfiore, G. Rekaya, and E. Viterbo. The golden code: a 2 × 2 full-rate space-time code with non vanishing determinants. IEEE Trans. in Information Theory, vol. 51, no. 4, pp. 1432–1436, Apr. 2005

[14] IST-2003-507581 WINNER. WINNER II Deliverable D1.1.2: WINNER II Channel Models, September 2007.

[15] I. Kim, Y. Han, Y. Kim, and S.C. Bang. Sequence hopping cell search scheme for OFDM cellular systems. IEEE Transactions on Wireless Communications, 7(5):1483–1489, May 2008.

[16] Hlaing Minn, Vijay K. Bhargava, and Khaled Ben Letaief. A robust timing and frequency synchronization for OFDM systems. IEEE Transactions on Wireless Communications, 2(4):822–839, July 2003.

[17] Y. Nasser, J.-F. Hélard, M. Crussiere, and O. Pasquero. Efficient MIMO-OFDM Schemes for Future Terrestrial Digital TV with Unequal Received Powers. in Proc. of IEEE International Communications Conference, May 2008, Bejing, China

[18] Timothy M. Schmidl and Donald C. Cox. Robust frequency and timing synchronization for OFDM. IEEE Transactions on Communications, 45(12):1613–1621, December 1997.

[19] F. Tosato, and P. Bisaglia. Simplified Soft-Output Demapper for Binary Interleaved COFDM with Application to HIPERLAN/2. Proc of IEEE Int. Conf. on Communications, pp. 664-668, 2002.

[20] Y. Tsai, G. Zhang, D. Grieca, F. Ozluturk, and X. Wang. Cell search in 3GPP long term evolution systems. IEEE Vehicular Technology Magazine, 2(2):23–29, June 2007.

[21] EU-IST FP6 Project Wireless World Initiative New Radio (WINNER). http://www.ist-winner.org.